Journal of Polymer Research (2018) 25: 106
https://doi.org/10.1007/s10965-018-1496-4

ORIGINAL PAPER

Synthesis and characterization of conjugated and nanostructured poly(propargyl alcohol) polymers

Atef A. Abdel-Fattah[1] · Yasser S. Soliman[1] · M. M. Ghobashy[1]

Received: 25 August 2017 / Accepted: 7 March 2018 / Published online: 28 March 2018

Abstract

New types of π-conjugated and colored poly(propargyl alcohol) polymers (poly-PGA) were prepared by the polymerization of propargyl alcohol (PGA) monomer in different media under the action of high energy photons, γ-rays, without the use of catalysts. The polymerization conditions depend on the used solvents (water, chloroform and dimethylformamide) and gases (O_2 and N_2). A singlet and broad electron paramagnetic resonance signal was observed in poly-PGA polymers, indicating the presence of free electrons and the delocalization of electrons through the polymer π-backbone. The synthesized polymers have FTIR bands (C=C) in the range of 1607–1652 cm^{-1} and an absorption broadband in the spectrum range of 305–316 nm. The poly-PGA polymers which synthesized in chloroform and DMF exhibited amorphous structures as approved by XRD results. In addition, both TEM and DLS measurements showed the formation of nanostructured polymers in the shape of nano-spheres, nano-stars and nano-networks depending on polymerization conditions. Radiation polymerization of the monomer in chloroform produced a polychlorinated polymer as demonstrated by EDX analysis. The polymers have optical band gaps in the range of 2.85–3.50 eV and conductivity in the range of 2.45×10^{-6} to 9.43×10^{-7} depending on the polymerization conditions and the media used.

Keywords Radiation polymerization · Nanostructures · Functional polymers · Polyacetylenes · Semiconductor

Introduction

Conjugated polymers are macromolecule compounds having π-electron conjugation in their backbone and are gained interests due their application in electronic devices and biomedical scopes [1–5]. Polyacetylenes (PAs) are a class of π-conjugated polymers possessing different applications [6] such as humidity sensors, ion-conducting polymer [7] and proton conducting polymer in solid-state battery [8]. The nano size and low toxicity of PA have actually been demonstrated in a wide range of in vitro sensing and cellular imaging [9], actuators [10]. Previous studies were concerned with the measurement of electrical conductivity of PAs depending on the π-bond percent as cis and trans isomers in the polymer chains; where the trans isomer is more conductive than cis isomer [11, 12]. PAs are types of semiconducting polymers and their conductivity was enhanced over many orders of magnitude in the case of iodine doping [13, 14] and is enhanced by treating with acid [8, 15] for use in the humidity sensors or in the battery constructions.

Many previous studies have been performed in the area of acetylene polymerizations by different methods. Almost the polymerization of acetylene (conducting) polymers in the form of solid film [16, 17] was carried out with various techniques to form thin film on Palladium surface [18] or by inductively coupled plasma reactor [19, 20] or copolymerized with another polymers [21]. PAs can be also synthesized with high molecular weight by polymerization of parent alkynes monomers with transition metal catalysts [22–25]. Propargyl alcohol (PGA) was previously polymerized by molybdenum catalyst on polyethylene and ruthenium complexes [26]. The obtained Poly(PGA) in this case is poor soluble in organic solvents. However, it was used as a proton-conducting polymer in solid battery constructions [8].

Gamma-radiation is an applicable source of energy for initiating polymerizations of arenes and alkenes [27, 28] and for modifying mechanical and optical properties of some polymeric materials [29, 30]. The most comprehensive study on radiation polymerization of alkyne was performed for many

✉ Yasser S. Soliman
yasser_shabaan@hotmail.com

[1] National Center for Radiation Research and Technology (NCRRT), Atomic Energy Authority (AEA), 3-Ahmad el-Zomor St, P.O. Box 8029, Nasr City, Cairo, Egypt

acetylene derivatives since 1962 [31]. Among the studied alkynes were propiolic acid and phenyl acetylene that exhibited the most radiation sensitivity and yields, %. The polymerization of acetylene in both liquid and solid state by gamma rays was reported [32]. The structure of PAs obtained is quite different in both cases. The color of the obtained polymer in the liquid-state was a relatively bulky orange-yellow, while; the color of the polymer in the solid-state was deep brown and insoluble in almost solvents. That is, the former obtained polymer is mainly *cis*-isomer and the latter is mainly *trans*-isomer. Radiation-induced synthesis of conjugated PAs type polymer was performed by solid-state polymerization of acetylenedicarboxylic acid at room temperature in normal atmosphere and under vacuum conditions, producing gray colored polymers [33]. The mechanism of polymerization was proposed to be a free radical mechanism. The obtained polymers were partially crystalline, exhibiting no melting up to 1200 °C. However, the polymer conversion rate is less than 5.5% at an absorbed dose of 500 kGy. Exposing phenyl acetylene to gamma radiation (320 kGy) in the presence of deoxycholic acid produced a trans type polyphenyl acetylene, but the yield was much lower [34]. Recently, Bassetti et al. [35] studied the radiation-induced polymerization of terminal aryl alkynes ($RC_6H_4C \equiv CH$) with different substituents. They exposed the monomers to gamma rays (50–400 kGy) in different organic solvents at room temperature. The methodology of using radiation in synthesis processes relies mainly on the basic of polymerization in transition metals catalyst-free environment. The obtained polymers are typically π-conjugated polyenes and soluble in organic solvents and can be obtained in micro/nanostructured size.

Self-assembly of conjugated polymer became an important topic of research to create various semiconducting nanostructures with high crystallinity [36, 37]. However, the self-assembly requires extensive optimization of the various post-synthetic treatments such as selective solvent additions, temperature modulation, or long-time aging. Thus, we produced a new radiation polymerization process to self-assembly the PPGA, such as polymerization-induced self-assembly [38, 39].

In this paper, we studied the synthesis of poly-PGA (PPGA) polymers at ambient conditions in different solvents (water, dimethyl formamide (DMF), and chloroform) and gases (O_2 and N_2) using gamma radiation as a metal-free polymerization method. The structures of PGA monomer and PPGA polymers were characterized by FTIR-ATR, UV-Vis spectroscopy, X-ray diffraction (XRD) and energy-dispersive X-ray (EDX) spectroscopy. The nanoparticle size was investigated by dynamic light scattering (DLS) and transmission electron microscope (TEM) analysis. In addition, the band gaps and electrical conducting property of the polymers were investigated. Free radicals formed in these polymers were also studied using electron paramagnetic resonance (EPR) spectrometer.

Experimental and method

Materials

Analytical grade solvents such as chloroform, dimethyl formamide (DMF), and PGA monomers (99%) were supplied from Sigma-Aldrich Co. Germany and used without further purification.

Synthesis of poly(propargyl alcohol)

To synthesize PPGA polymers, 25 ml of PGA monomer was selected at each condition of polymerizations. Seven glass bottles containing 25 ml of PGA were prepared and assigned as b to h (see Table 1). The monomer without any additions and treatment was assigned a. Bottle b has a pure monomer without any additions and bottle c contains PGA monomer saturated with O_2 molecules. While, bottles d, g, and h contain 25 ml of water, chloroform and DMF, respectively added to the pure monomer, 25 ml. Meanwhile, bottle e has only the monomer saturated with N_2 gas while f contains 1/1 (v) water to monomer saturated with N_2 gas. After that, bottles (b to h) was irradiated by gamma radiation at the center of irradiation facility chamber at 190 kGy. After the end of γ-irradiation, all solutions were left for drying at room temperature under vacuum to vaporize the solvents then were placed in the oven (40–45 °C) for complete drying. After complete drying process, the obtained polymers were washed with distilled water, filtrated, and dried in oven (40 °C). The physical and chemical properties of the obtained polymers were further studied.

Irradiation facility

Gamma-radiation polymerization of PGA monomer was performed using ^{60}Co Gamma Cell 220 Excel (manufactured by MDS Nordion, Canada). Irradiation process was performed in the central position of the gamma cell chamber. The dose rate equals to 1.40 kGy/h at the time of this experiment as calibrated by the transfer standard alanine dosimeter of the National Physical Laboratory (NPL), UK; thus the calibration is traceable to NPL. The overall uncertainty of the absorbed dose rate was ±2.4% (95% confidence level).

Measurements and analyses

The attenuated total reflectance (ATR) of PGA monomer and the synthesized PPGA polymers were investigated using FTIR spectrometer (Vertex 70, Bruker Optik Gmbh, Germany) equipped with platinum diamond ATR crystal. A UV-Vis spectrophotometer, Evolution 500 type (Thermo Electron Corporation, England) was used to investigate the UV-Vis spectra of PGA monomer and PPGA polymers. The monomer sample was investigated in a quartz cuvette by

Table 1 Polymerization conditions of PGA monomer irradiated at an absorbed dose of 190 kGy

Sample no	PGA (%)	Gas bubbling	Solvent	Sample Key	Polymers color
b	100	Absent	Absent	PPGA	Orange
c	100	O_2	Absent	PPGA-O_2	Deep orange
d	50	Absent	Water	PPGA-W	Orange
e	100	N_2	Absent	PPGA-N_2	Orange
f	50	N_2	Water	PPGA-NW	Orange
g	50	Absent	Chloroform	PPGA-Ch	Shiny Black
h	50	Absent	DMF	PPGA-DMF	Reddish brown

PGA pure monomer without irradiation is assigned as (a)

adding two drops of monomer on the wall of the cuvette. The polymer samples were measured as thin films coated on glass plates.

To study the free radical formed in the polymers, the EPR spectra were recorded at room temperature using an X-band EPR (EMX, Bruker) equipped with a standard rectangular cavity of ER 4102. The operating parameters adopted throughout the experiment are: central field, 3460.41 G; microwave frequency, 9.71; microwave power, 2.012 mW; modulation amplitude, 5 G; modulation frequency, 100 kHz; time constant, 81.92 s; sweep time, 20.972 s; receiver gain, 7.96×10^3. The X-ray diffraction (XRD) patterns of PPGA polymers in a powder form were also analyzed at room temperature by a Shimadzu X-ray diffractometer (XRD-6000 model, 40 kV, 30 mA) equipped with X- ray tube (Cu target). The X-ray diffractometer is a product of Shimadzu Scientific Instruments (SSI), Kyoto, Japan. The X-ray data were recorded with continuous scanning mode and scanning speed 8 (deg/min) in the range of 4^o-90^o (2θ).

Dynamic Light Scattering (DLS) of the obtained polymer solutions were analyzed using a Nicomp 380 ZLS Submicron Particle Size Analyzer (Product of 8203 Kristel Circle Port Richey FL, 34668, pssnicomp, USA) to obtain the particle size distribution of the samples with particles ranging from 0.002–5 μm at the scattering angle of 90° after diluting samples with deionized water. The sample volume used for the analysis was kept constant i.e. 2 ml to nullify the effect of radiation strays from sample to sample. Prior to sample loading, glass vessels were thoroughly cleaned, washed with deionized water, and dried. The measurements were repeated at least three times at room temperature and the standard deviation (SD) was calculated using the software. A transmission electron microscope (TEM) type Jeol JEM-100CXII (JEOL Ltd. 1–2, Musashino 3-chome Akishima Tokyo 196–8558, Japan) was also used to analyze the nanoparticle size of PPGA polymers. The TEM used is a 100 kV with a tungsten electron source with holder capable of taking three 3 mm specimens and the resolution is 0.2 nm lattice, 0.45 nm point-to-point. The samples were prepared by placing a drop of solution on a carbon coated copper grid and allowing the grid (200 mesh) to dry on filter paper and examined with resolution: 0.3 nm; magnification: × 330 to 250,000; Specimen thickness 150 nm. The average size of PPGA nanoparticles was determined from the TEM images using the Image J software..

The EDX analyses of PPGA polymers were examined with JED-2300 Analysis Station™ (JEOL Ltd. 1–2, Musashino 3-chome Akishima Tokyo 196–8558, Japan. Electrical conductivity measurements were performed for the pressed discs of PPGA. These samples were place in a cell with brass electrodes in the temperature range of 295–315 K, using an electric heater in isolated chamber and a thermocouple placed very close to the sample. For the dc conductivity measurements, a Keithly-617 electrometer was used for measuring resistance of the pressed discs at different temperatures within the range of 295–315 K.

Results and discussions

FTIR-ATR analysis

ATR spectra of PGA monomer and PPGA polymers powder generated upon irradiating the monomer in different conditions are shown in Fig. 1(a–h). Figure 1a shows the ATR characteristic peaks of PGA monomer. As shown from Fig. 1a, the bands at 3350 cm^{-1} and 3288 cm^{-1} are characteristics of O–H and ≡C–H terminal (sp C-H stretch), respectively. This spectrum displays a band at 2120 cm^{-1} which attributed to C ≡ C stretching vibration and bands of 2923 cm^{-1} and 2871 cm^{-1} assigned to C–H stretching of CH_2 group. Bands of C–O and ≡C–C with strong intensity appear at 1020 cm^{-1} and 922 cm^{-1}, respectively [40]. While the band corresponding to ≡C–H bending for PGA monomer appeared at 636 cm^{-1}. As shown from Fig. 1a to h, the intensity of ≡C-H stretching frequency of the polymers decreases significantly and another two bands characteristics of C=C develop in the range of 1653–1607 cm^{-1} from b to h, indicating the radiation polymerization of PGA monomer. In DMF samples (h) only, two strong peaks appear at 1653 cm^{-1} and 1626 cm^{-1} and the other polymer samples the C=C peaks are weak, indicating higher conjugation in this polymer backbone. The spectrum band at

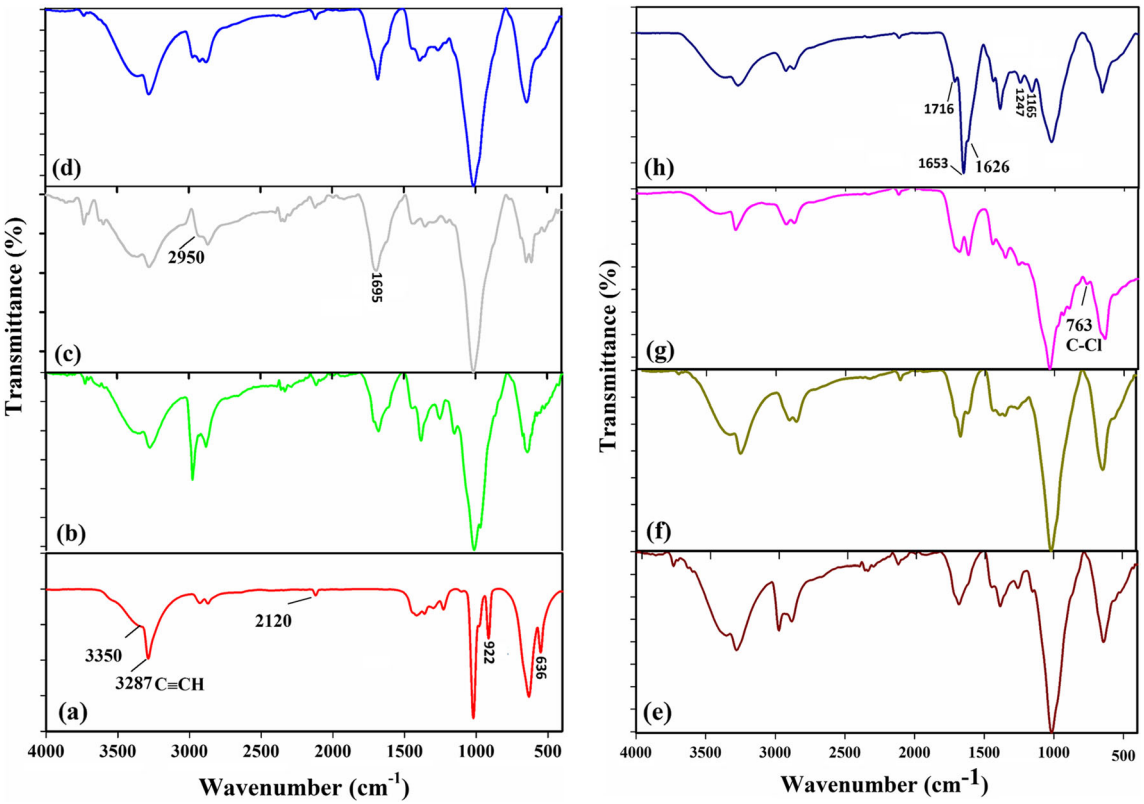

Fig. 1 FTIR-ATR spectra of PPGA polymers powder prepared by different polymerization conditions

2120 cm^{-1} of C ≡ C decreases also greatly in most cases after polymerizations. The presence of two bands of ≡C-H and C ≡ C indicates the polymer terminal structure. Furthermore, the monomer's bending band of ≡C–C (922 cm^{-1}) nearly disappears in the synthesized polymers (b-h) and the intensity of ≡C–H bending bands (636 cm^{-1}) decreases significantly. In the polymers, OH band (3350 cm^{-1}) is broad, which is indicative of the strong H-bonding in the polymers. FTIR spectra (Fig. 1c) of PPGA-O_2 displays two absorption bands at 1695 cm^{-1} and 1713 cm^{-1} assigned to C=O [18, 25], indicating the oxidation during polymerization process. Bands in the range of 1679–1716 cm^{-1} characteristics of C=O are also observed in the case of using water (Fig. 1d), water-N_2 (Fig. 1f), and DMF (Fig. 1h). In addition, these bands appeared with low intensity for the samples of PPGA-N_2 (Fig. 1e), and PPGA-Ch (Fig. 1g).

$$-CH=CH- + 1/2O_2 \rightarrow {}^{-CH=C-}_{\quad\;|}{}_{\quad OH} \rightarrow {}^{-CH_2-C-}_{\quad\quad\;\|}{}_{\quad\quad O}$$

In PPGA-DMF sample, a strong peak at 1716 cm^{-1} appeared, which may be assigned as C=O of COO^- formed in the polymer backbone. This may be supported by the two peaks located at 1247 cm^{-1} and 1165 cm^{-1} which can be attributed to the coupling between C-O and OH in-plane [41, 42]. Figure 1g (PPGA-Ch) displays a band at 763 cm^{-1} assigned to C–Cl bond, indicating the formation of chlorinated PPGA polymer [43]. A radiolysis of CHCl3 releases Cl- ions then the ions abstract hydrogen from the medium forming HCl [18, 44, 53] that can interact with the polymer backbone forming polychlorinated polymers. Thus, the polymerization, in this case, may proceed by the cationic mechanism by the action of hydrogen chloride formed by CHCl3 radiolysis. Propargyl chloride can be obtained from chlorination of PGA [45]. Radiation-induced ionic (cationic or anionic) polymerization is controlled by the presence of Lewis acids or Lewis bases [46]. On the other hand, the radiolysis of DMF causes the formation of fragmented ions ($^{\bullet}N(CH_3)_2$, $^{\bullet}CH_2=N$ and $^{\bullet}CHO$) by the capture of solvated electrons, evidently the formation of radical anion [47–50]. $^{\bullet}CHO$ could attack the polymer backbone and with further irradiation, it might be oxidized to form COOH as supported by the strong peak at 1716 cm^{-1}. It may be proved also by the appearance of two peaks of 1247 cm^{-1} and 1165 cm^{-1} that assigned to the coupling between C-O and OH in plane [41, 42]. Thus, the conjugation cannot be altered in this case. The polymerization of PGA in DMF may be not initiated mainly by anionic polymerization but by a dual radical-anionic mechanism. This mechanism was previously proposed by Tsuda (1962) [51].

Regarding the radiolysis of chloroform by gamma radiation, chloroform may act as Lewis acid with the monomers

having a Lewis base character. The radiolysis of chloroform under effect to gamma radiation as follows.

$$CHCl_3 + e^- \rightarrow CHCl_2 + Cl^- \quad (1)$$

Due to electron capture, the abundant yield of chloroform radiolysis is chloride ion [52]. This electron may be released from irradiated $CHCl_3$ molecules [53].

$$CHCl_3 \rightarrow CHCl_3^+ + e^- \quad (2)$$

Or the electron may be released from π-electron rich monomer (donor), acting as Lewis base to the suitable solvent acceptor that acting as Lewis acid. This will lead to initiation of cationic polymerization [54].

On the other hand, the irradiated DMF decomposes as follows [55, 56].

$$HCON(CH_3)_2 \xrightarrow{\gamma} HCON(CH_3)^*_2 + HCON(CH_3)_2^+ + e^- \quad (3)$$

In general, both the cationic and anionic radical polymerization induced by gamma radiation are controlled by the monomer type act as Lewis base and Lewis acid, respectively [46].

UV-vis. spectra of PPGA polymers

The UV-Vis spectra of various PPGA polymers were inspected in the spectrum range of 200–600 nm as shown in Fig. 2. To inspect the polymers in the spectrophotometer, they were dissolved in DMF, casted onto glass slides to form thin solid films and then dried. The absorption band of the monomer is located at $\lambda_{max} \approx 202$ nm. While the absorption bands of PPGA polymers formed upon irradiating the monomer are located at λ_{max} ranging from 305 to 316 nm. All those bands are broader than the peak of PGA monomer, indicating the delocalization of π-conjugated electrons in the polymers. Highly intense absorption bands in the region from 280 to 410 nm are due to $\pi \rightarrow \pi^*$ transition for all polymer types [51, 57, 58]. These absorption bands are characteristic of π-conjugated polymers and arise from the delocalization of electron in double bonds alongside the polymer chains, causing the broadening and shifting of the maximum absorption [59–61]. A lower energy broad band centered at 410 nm is observed only for PPGA-DMF, suggesting a longer conjugation length [61] as supported by ATR-FTIR spectra in the two strong bands at 1626 $cm^{-1}$and 1652 cm^{-1}. The obtained results of UV-Vis spectra of these polymers are nearly comparable with the results of poly(propargyl ester), which absorbs in the range of 300 nm to 425 nm [61]. The polymers absorbed at wavelength greater than 400 nm are that possessing longer conjugation chain [62]; this as in the case of PPGA-DMF samples. The optical energy band gaps (*Eg*) for the samples were estimated from the intercept of the linear portion of the plot $((\alpha h\nu)^2$ versus $h\nu)$ at $(\alpha h\nu)^2 = 0$ using Tauc relation [63, 64]. Where α, h, and ν are the absorbance, Planck's constant, and the frequency of light, respectively. The optical band gaps for pure PPGA, -O_2, -W, -N_2, -NW, -Ch, -DMF are 3.39, 2.78, 3.57, 3.50, 3.40, 3.4 and 2.85 eV, respectively.

EDX analysis of PPGA polymers

The EDX profiles of synthesized PPGA polymers are conducted as shown in Fig. 3. EDX profile, PPGA-Ch confirms the presence of chlorine atoms in the polymer prepared in chloroform solvent, agreeing with the FTIR results. The amount of Cl in PPGA-Ch is 39.5% on comparing with the amount of carbon in the polymers, indicating the formation of highly chlorinated-poly(PGA). Oxygen content in PPGA-Ch per C content is 30.56%, indicating an oxygen decrease in the polymer by 2.72% on comparing with oxygen content in the monomer before treatment. In the other two polymers, PPGA-W and PPGA-DMF, O content/C content is 48.12% and 73.3%, respectively. This means that the oxygen content increases from the initial monomer by ~14.8% and ~40%, respectively, implying the higher oxidation in the polymers backbones especially in case of DMF polymerization that consistent with FTIR-ATR results.

XRD analysis of PPGA polymers

Figure 4 displays the X-ray diffraction of PPGA prepared at various conditions. The XRD pattern of PPGA-W exhibit three diffraction peak; the first one is sharp at $2\theta = 16.75°$, the second main peak is broad at 22.37° (interplanar distance d = 3.97 Å), and the third peak is very broad at 40.75°. This means that this polymer has both amorphous and crystalline regions, which may be related to oxidation on π-conjugated backbone. While the XRD pattern of PPGA-Ch exhibits two peaks at $2\theta = 24.27°$ (d = 3.66 Å) and small one 44.97° (d = 2.01 Å). These values are very close to an amorphous natural graphite; the interplanar spacing of graphite d_{002} is ranging from 3.58 to 3.66 Å and d_{100} is 2.03 Å for peaks of $2\theta = 24°$ and 44° [65], respectively. This means that the PPGA-Ch is nearly graphite like structure. The same phenomenon was noted by Geiss and his coworkers whose founded that the XRD chart of polypyrrole is similar to the XRD peaks of graphite [66]. The XRD chart of PPGA prepared in DMF solvent (PPGA-DMF) displays a broad peak centered at 20°, indicating the complete amorphous nature of this polymer. The ratio of the half-height width to diffraction angle ($\Delta 2\theta/2\theta$) of the synthesized polymers is greater than 0.35, indicating that the synthesized polymers are amorphous [67–69]. The broad peaks in the polymers, approximately at $2\ \theta = (20–24\ °C)$ are due to the intermolecular internal $\pi \rightarrow \pi^*$ stacking [70].

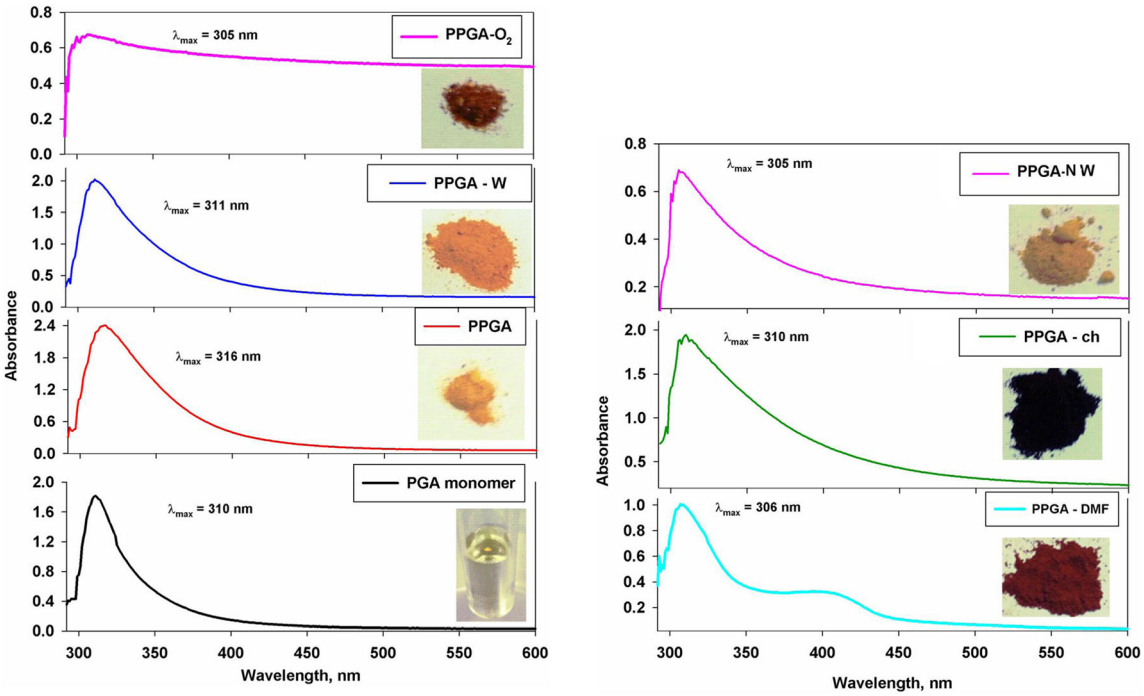

Fig. 2 UV-Vis. spectra of PPGA nanostructure prepared by different polymerization conditions

EPR spectra and free electrons formation

It is well known that many, if not all, conjugated polymers display paramagnetic centers with a spectroscopic splitting factor (g-factor) close to the free-electron (2.0023) [71]. The electron paramagnetic resonance (EPR) spectra of radiation-synthesized PPGA polymers at room temperature are shown in Fig. 5. Obviously, all PPGA polymers have a symmetrical, isotropic and singlet EPR signal, indicating the formation of one free radical center, neutral defect, in the polymer. The free radical formed is referred to a neutral soliton, a localized unpaired electron, which could enhance the conductivity through the polymer π-conjugated backbone [67]. Previous studies give an evidence of the presence of mobile, uncharged, paramagnetic defects in un-doped and lightly doped PAs that is called as a soliton and proposed as a model for the defect [72, 73]. Table 2 summarizes the results of EPR measurements of the prepared polymers. It seems that g-factors of the polymers are depending on the polymerization conditions and their values are nearly close to the g-factor of free electrons. The intensity of radicals, number of spin, of PPGA-Ch possessed higher intensity of EPR signal indicating the higher number of spins. On comparison with PPGA, the EPR intensity of PPGA-Ch is higher than PPGA by 390%. The EPR signal intensity of the PPGA is nearly the same as PPGA-O_2 while PPGA-W possesses a lower EPR signal. The higher peak width (ΔH) values suggest that the unpaired electrons highly delocalize through the π-conjugation of polymer backbone [74]. Thus, PPGA-N_2 polymer possesses the highest delocalization among the tested polymers. This may be attributed to that the polymerization under N_2 atmosphere did not disturb the conjugation chain in the polymer backbone.

TEM analysis of PPGA polymers

Self-assembly polymer nanosize preparation, termed the 'in situ nanoparticlization of conjugated polymers' (INCP), was derived by utilizing a conjugated polymer with high strong π–π interactions [75, 76]. In situ nanoparticlization of fully conjugated block copolymers containing PA and endo-tricyclo[4.2.2.0]deca-3,9-diene (TD), they spontaneously form nanospheres consisting of a PA core and PTD shell, but their electronic application was rather limited, mainly attributed to the low conductivity of the synthesized shell [77]. Herein, we announce the formation of different nanostructures from PPGA polymers depending on the polymerization conditions. Figure 6 displays the TEM images of PPGA-W, PPGA-Ch, and PPGA-DMF polymers. PPGA-Ch image displays irregular spheres in nanosize ranging from 5 nm to 70 nm. The morphology of PPGA-Ch with irregular sphere particles may be attributed to the repulsion occurred among chlorine atoms attached in the polymer chain. On the other hand, PPGA nanoparticles as one-dimensional (1D) rods and long-branching nanoparticles forming nanostar and nanonetwork appeared in PPGA-DMF and PPGA-W, respectively. The formation of nanostructures in PPGA-DMF and PPGA-W might be attributed to the spheres was expanded and clung to others, based to solvation and polarity of function groups

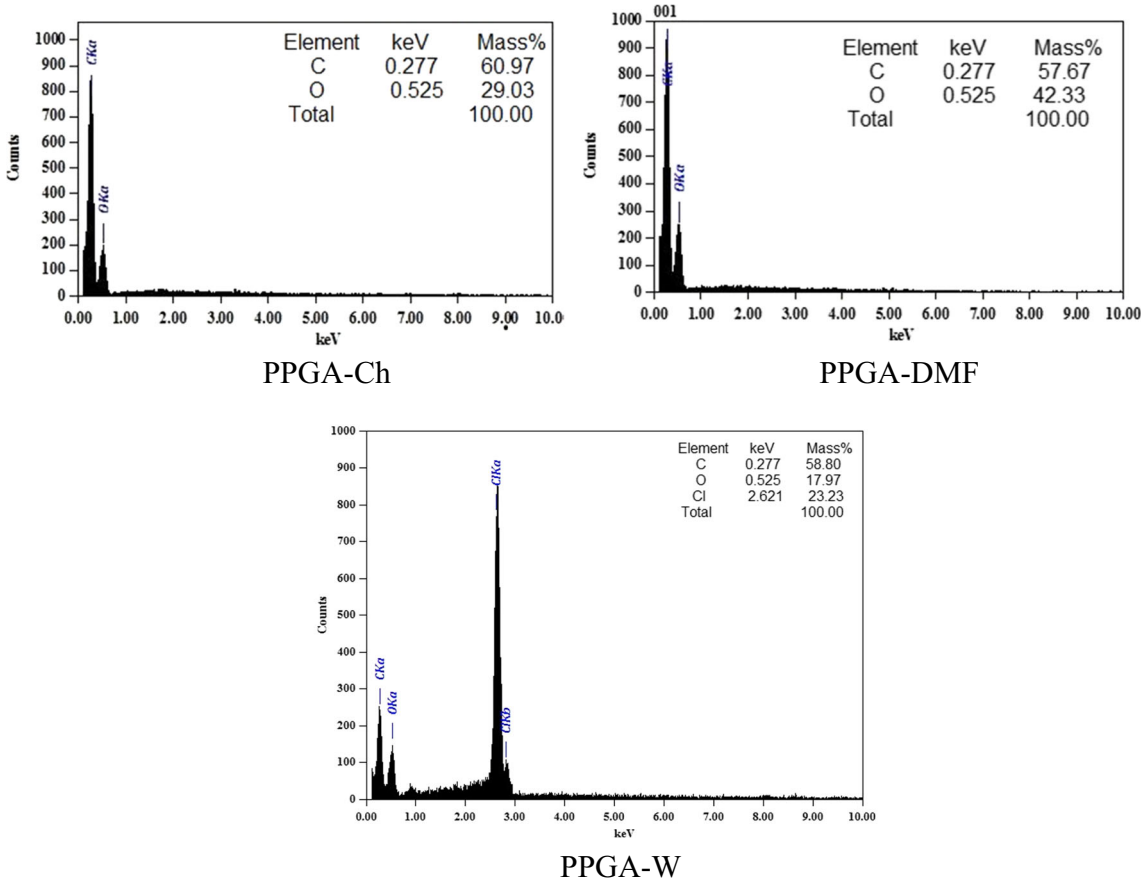

Fig. 3 EDX analysis of PPGA-W, PPGA-Ch and PPGA-DMF

thereby forming the nanostar and nanorods, driven by strong interactions between the spheres of PPGA as shown in Scheme 1. Thus, these methods of preparations produce in situ self-assembly conjugated PPGA polymers. PPGA-DMF polymer mostly exhibits the formation of star-shaped nanostructure (nanostar), exhibiting a little branching through the π-conjugation polymer backbone. The height of the nanostar on this type is 20–50 nm with 2 nm diameter. Nanonetwork structures were observed in TEM image (Fig. 6c) for PPGA-W, indicating the crosslinking of the polymer backbone. The nanonetwork has the largest fibril shape with more than 1 μm and small fibril diameter about 2–4 nm. Nanonetwork structures are formed by that the nano-spheres are coming nanoneedles, which in their turn, are collected in order to create nanostars, which are further connected together for the formation of nanonetworks as schematically presented in Scheme 1 depending on the suggestion was recorded by authors [74, 78]. Moreover, the dynamic light scattering (DLS) analyzed the hydrodynamic diameter as seen in Fig. 7. DLS identifies the hydrodynamic diameter (D_H) of the PPGA nanostructure powder dispersed in bi-distilled water. D_H for PPGA-W, PPGA-DMF, PPGA-Ch was 1550 nm, 120 and 139 nm, respectively that is in the agreement with TEM images.

According to the supporting data, we demonstrated the formation of PPGA nanostructures. They were produced by an extremely simple method for the self-assembly of conjugated polymer PPGA by gamma radiation (Scheme 1). The conjugated polychlorinated polymer, PPGA-Ch appeared in a nanosphere structure upon radiation polymerization in chloroform. The interaction between Cl atoms may cause repulsion among PPGA particles, forming separated particles as indicated by TEM analysis. Strong π-π interactions of the conjugated PPGA-DMF, as the driving force for self-assembly, imply that the particles are queue to form nanoneedles that in most case have nanostar morphology. The interconnection of PPGA-W nanospheres induces a formation of nano networks. This may related to strong interaction obtained due to hydrogen bonding among the polymer molecules.

Evaluation of PPGA polymer types as semiconductors

Table 3 shows the conductivity, $\Omega^{-1}.cm^{-1}$ of all synthesized polymers. It was observed that the conductivity values and energy band gaps indicates the semiconducting property of the prepared polymers. Surprisingly, PPGA-DMF polymer exhibited higher conductivity (2.45 ×

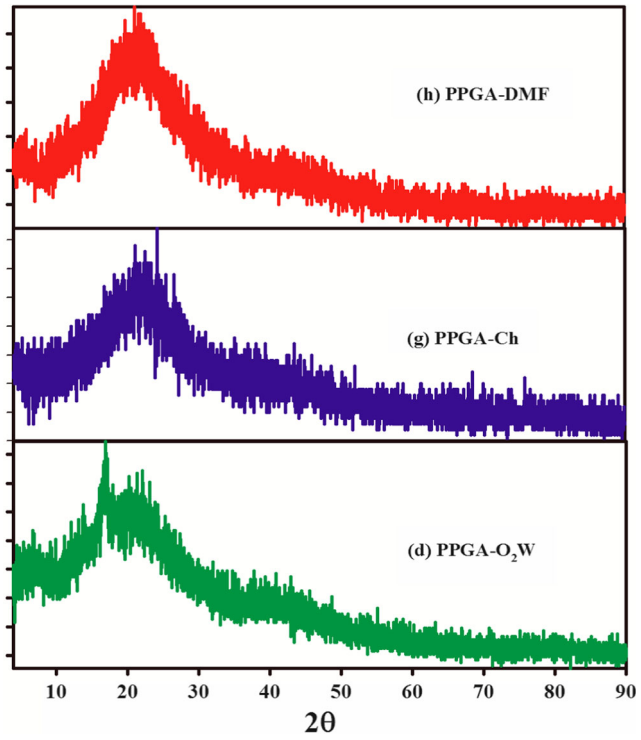

Fig. 4 XRD of PPGA polymers (PPGA-W, PPGA-Ch and PPGA-DMF)

10^{-6} Ω^{-1}.cm^{-1}) although it presented higher oxidation in its conjugation chain. This may be attributed to that the oxidation occurred by attaching •CHO on the polymer chain as C–C–CHO not by a direct oxidation as C–C=O and the coupling between C=O and OH groups is in plane as approved by FTIR-ATR in Fig. 1h (see "FTIR-ATR Analysis" section). This could facilitate the transportation of the electrons through the polymer chain not to restrict the flow of electrons.

Table 2 g-factors and band width of EPR spectra of PPGA polymers

Polymer type	g factor	ΔH, G
PPGA	2.0095	9.99
PPGA-W	2.0088	9.83
PPGA-N_2	2.0090	10.92
PPGA-O_2	2.0086	9.83
PPGA-Ch	2.0080	8.00
PPGA-DMF	2.0089	8.44

In addition, the charge generation through temperature rise has been investigated for PPGA-Ch sample. Figure 8 displays the effect of temperature on electrical conductivity. As expected the temperature enhances the electrons mobility (freedom to move) through a polymer chain, increasing the conductivity with the temperature rise. Increasing the temperature from 25 to 40 °C enhances the conductivity from 1.11×10^{-6} to 2.5×10^{-4} Ω^{-1}.cm^{-1}. This behavior is similar to the semiconducting materials.

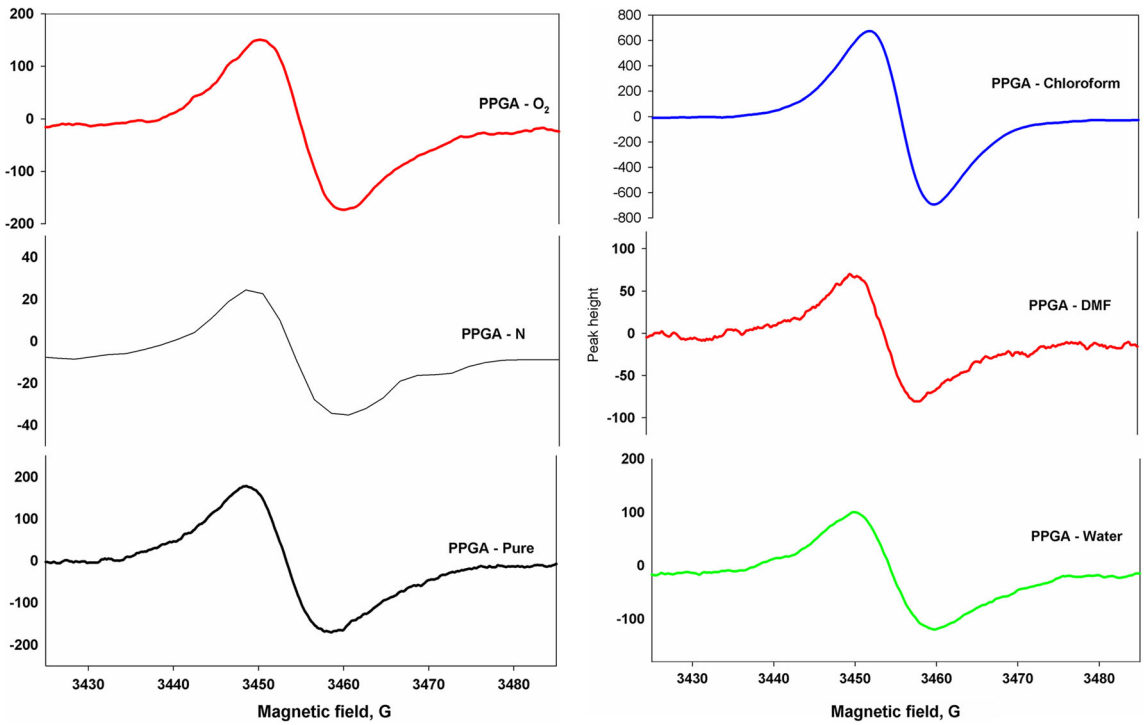

Fig. 5 EPR spectra of all prepared polymers

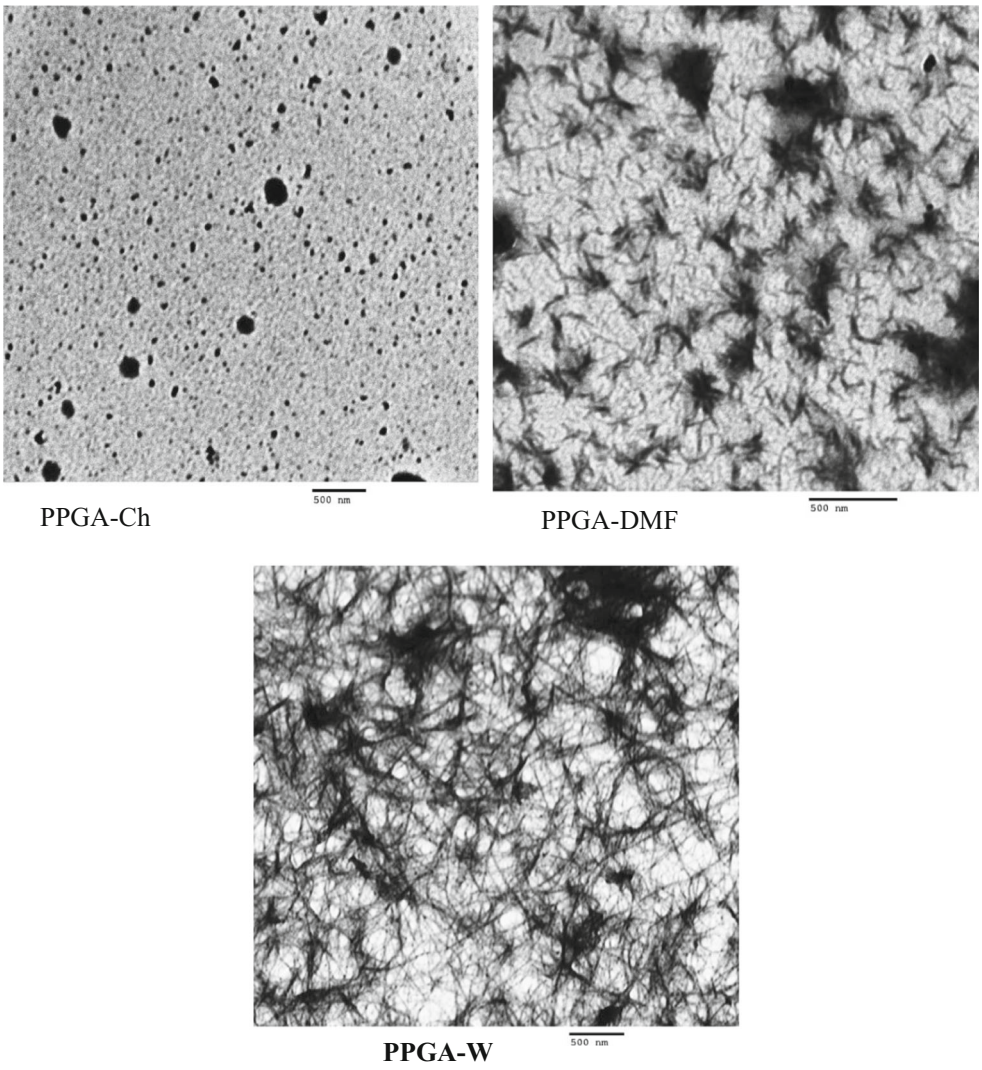

Fig. 6 TEM image of self-assembled structures formed by polymerization of PGA in a) Chloroform, b) DMF and c) Water to produce PPGA-Ch, PPGA-DMF and PPGA-W, respectively

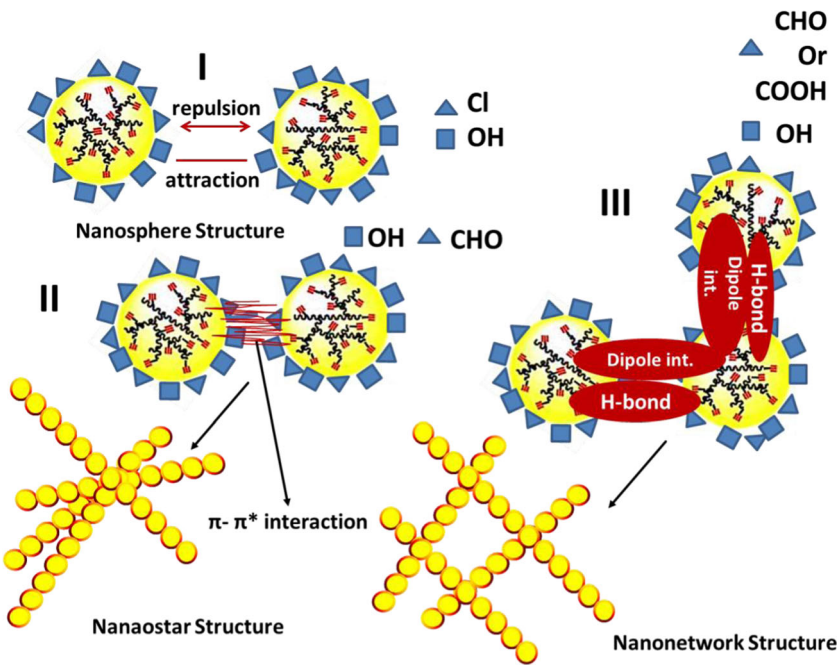

Scheme 1 Proposed mechanism of the formation different nanostructure particles of PPGA polymers, (I) PPGA-Ch, (II) PPGA-DMF, and (III) PPGA-W

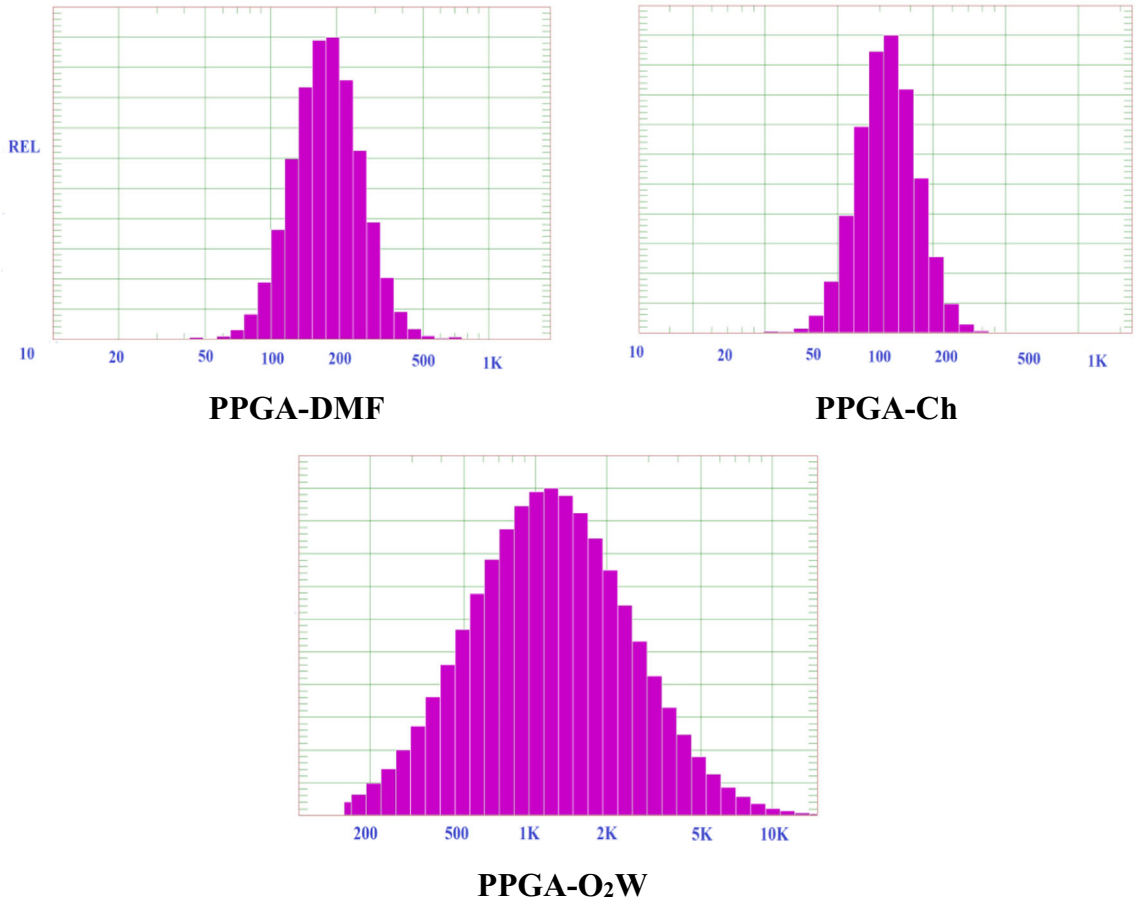

Fig. 7 DLS profiles of PPGA nanostructure particles suspend in water

Conclusion

PGA monomer undergoes polymerization reaction upon exposure to γ-radiation, forming highly π-conjugated and yellow colored PPGA polymers. PPGA polymers nanostructures are organized via choosing the appropriate solvent. In the absence of surfactant, PPGA types forms self-assembly nanospheres or nanostars or nanonetwork structures depending on the solvent that can act as initiator and make a great effect on the kind of polymerization mechanism. Thus, the polymerization conditions could control the morphology of nanostructure. According to TEM image, PGA polymerized in DMF solvent exhibits extensive and short nanostar shape (2–5 nm). The interconnection of the nanospheres was responsible for the formation of nanostar and nanonetwork structures in DMF and water solution, respectively. Meanwhile, the polychlorinated polymers possess nanosphere structures (5–70 nm). The data

Table 3 Conductivity measurements of PPGA polymers

Polymer type	Conductivity, Ω^{-1} cm^{-1}
PPGA	2.32×10^{-6}
PPGA-W	9.43×10^{-7}
PPGA-N_2	1.11×10^{-6}
PPGA-NW	1.56×10^{-6}
PPGA-O_2	4.95×10^{-7}
PPGA-Ch	1.11×10^{-6}
PPGA-DMF	2.45×10^{-6}

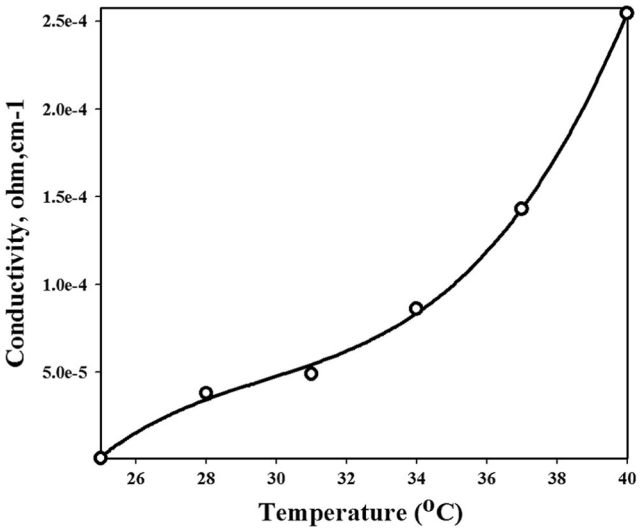

Fig. 8 Conductivity of PPGA-Ch with temperature change

acquired from XRD analysis confirm the amorphous structure of all polymer types.

ATR-FTIR analysis confirms the radiation-induced polymerization of PGA by forming C=C, decreasing the stretching vibration of C ≡ C and H-C ≡ C, and disappearing the bending vibration of ≡C–C. However, the bands of C ≡ C and H-C ≡ C stretching are still present, indicting the terminal structure of PPGA polymers. The PGA monomer has an absorption band at $\lambda_{max} \approx 202$ nm. Upon irradiation and polymer formation, highly broad bands from 305 to 316 nm appear, indicating the increase of π-electrons delocalization and conjugation along the polymer backbone. Only in the case of polymerization in DMF, a band at 410 nm is observed, indicating the higher conjugation through the polymer backbone. This may be attributed to that the oxidation that confirmed by ATR and EDX occurred by attaching $^{\bullet}$CHO on the polymer chain as C–C–CHO not by a direct oxidation on the polymer backbone as C–C=O. This group with continuing irradiation may be subjected to oxidation forming COO^{-}. This group acts as chromophore stabilizing the π-conjugation. It presents in the same plane of PPGA-DMF chain that could facilitate the transportation of the electrons through the polymer chain thereby it does not restrict the flow of electrons. The higher conjugation was also supported by the two strong ATR peaks of 1653 cm^{-1} and 1626 cm^{-1} (C=C). A sharp peak of C=O carboxylic appeared at 1716 cm^{-1} and two peaks located also appeared at 1247 cm^{-1} and 1165 cm^{-1} of the coupling between C-O and OH in-plane.

Polymerization in DMF introduces 40% oxygen more than the initial oxygen in PGA monomer on comparing with the carbon polymer content. Meanwhile, polymerization of PGA in chloroform produces highly polychlorinated PPGA polymers. Whereas the chlorine amount is 39.5% on comparing with the carbon content in the polymers. However, the oxygen content in PPGA-Ch is less than the initial oxygen of PGA by 2.7%. On the other hand, polymerization in water or DMF introduces greatly oxygen in the polymers; the oxygen content of these polymers increases by ~14.8% and ~40%, respectively on comparing with the initial oxygen of PGA monomer. All PPGA polymers possess a paramagnetic center, free electrons, along the backbone of the polymer. In addition, they display great broad EPR signal, indicating the higher delocalization of free electrons in consistence with UV-Vis. spectra. The optical band gaps are varied from 2.85 eV to 3.50 eV. The conductivity of the synthesized polymers is varied from 2.45×10^{-6} to 4.95×10^{-7}, indicating the semiconducting property of the polymers. The DMF polymer samples show the highest conductivity value (2.45×10^{-6}) among PPGA polymers that may attributed to higher conjugation produced in the PPGA-DMF sample that confirmed by the ATR spectra, Vis-spectra, and lower conduction band. The conductivity of chloroform polymer samples (1.11×10^{-6}) are comparable with the nitrogen polymer samples. The conductivity of the PPGA-Ch samples increases with increasing temperature, following a 2nd order function. In the future, the molecular weight variations, nuclear magnetic resonance, thermal behavior and thermal stability as well as the microbial activity will be studied.

Acknowledgements We would like to thank and appreciate Dr. Seth C. Rasmussen (Professor - Materials Chemistry and Chemical History, Department of Chemistry and Biochemistry, Materials and Nanotechnology Program, North Dakota State University) for his guidance and valuable information he has provided on the manuscript.

References

1. Feng X, Liu L, Wang S, Zhu D (2010) Water-soluble fluorescent conjugated polymers and their interactions with biomacromolecules for sensitive biosensors. Chem Soc Rev 39:2411–2419
2. Duarte A, Pu K-Y, Liu B, Bazan GC (2011) Recent advances in conjugated polyelectrolytes for emerging optoelectronic applications. Chem Mater 23:501–515
3. Thomas SW, Joly GD, Swager TM (2007) Chemical Sensors Based on Amplifying Fluorescent Conjugated Polymers. Chem Rev 107: 1339–1386
4. McQuade DT, Pullen AE, Swager TM (2000) Conjugated Polymer-Based Chemical Sensors. Chem Rev 100:2537–2574
5. Liu J, Geng J, Liao L-D, Thakor N, Gao X, Liu B (2014) Conjugated polymer nanoparticles for photoacoustic vascular imaging. Polym Chem 5:854
6. Minto RE, Blacklock BJ (2008) Biosynthesis and function of polyacetylenes and allied natural products. Prog Lipid Res 47: 233–306
7. Casalbore-Miceli G, Yang MJ, Camaioni N, Mari C-M, Li Y, Sun H, Ling M (2000) Investigations on the ion transport mechanism in conducting polymer films. Solid State Ionics 131:311–321
8. Camaioni N, Casalbore-Miceli G, Martelli A, Yang MJ (1997) A novel solid state battery based on a polymer proton conductor: poly (propargyl alcohol) doped with perchloric acid. J Appl Electrochem 27:862–866
9. Li J, Liu J, Wei CW, Liu B, O'Donnell M, Gao X (2013) Emerging applications of conjugated polymers in molecular imaging. Phys Chem Chem Phys 15:17006–17015
10. Smela E (2003) Conjugated Polymer Actuators for Biomedical Applications. Adv Mater 15:481–494
11. Deits W, Cukor P, Rubner M, Jopson H (1981) Analogs of polyacetylene. Preparation and properties. Ind Eng Chem Prod Res Dev 20:696–704
12. Ito T, Shirakawa H, Ikeda S (1975) Thermalcis–trans isomerization and decomposition of polyacetylene. J Polym Sci A Polym Chem 13:1943
13. Shirakawa H, Louis EJ, MacDiarmid AG, Chiang CK, Heeger AJ (1977) Synthesis of electrically conducting organic polymers: halogen derivatives of polyacetylene, $(CH)_x$. J Chem Soc Chem Commun 0:578
14. Carlin C, Chien JCW (1984) Semiconducting poly(monocyanoacetylenes). J Polym Sci A Polym Chem 22: 2749
15. Yang MJ, Sun HM, Casalbore-Miceli G, Camaioni N, Mari CM (1996) Synth Met 65
16. Faria RM, Oliveira Jr ON (1999) Exploiting the electrical properties of thin films of semiconducting polymers. Braz J Phys 29:360–370
17. Skotheim TA, Reynoald JR eds (1997) Handbook of conducting polymers. CRC Press, page 205

18. Yang M, Zheng M, Furlani A, Russo MV (1994) A novel palladium catalyst for the polymerization of propargyl alcohol. J Polym Sci A Polym Chem 32:2709–2713
19. Fally F, Virlet I, Riga J, Verbist JJ (1996) Detailed multitechnique spectroscopic surface and bulk characterization of plasma polymers deposited from 1-propanol, allyl alcohol, and propargyl alcohol. J Appl Polym Sci 59:1569–1584
20. Hozumi K (1988) Plasma polymerization of unsaturated alcohols for deposition of hydrophilic thin film. Pure Appl Chem 60:697
21. Camaioni N, Casalbore-Miceli G, Li Y, Mari CM, Yang MJ (2001) Ion conductivity in poly(p-diethynylbenzene-co-propargyl alcohol) films doped with iron trichloride: dependence on temperature. Solid State Ionics 144:355–359
22. Liu J, Lam JWY, Tang BZ (2009) Acetylenic polymers: syntheses, structures, and functions. Chem Rev 109:5799–5867
23. Masuda T (2007) Substituted polyacetylenes. J Polym Sci A Polym Chem 45:165–180
24. Voronkov MG, Pukhnarevich VB, Sushchinskaya SP, Annenkova VZ, Annenkova VM, Andreeva NJ (1980) Polymerization of acetylene and its monosubstitutes in the presence of halides and oxohalides of molybdenum and tungsten. J Polym Sci A1 18:53–57
25. Yamaguchi I, Osakada K, Yamamoto T (1994) Ruthenium complex catalyzed polymerization of OH or COOH group containing alkynes to give functionalized poly(acetylene)s. lnorg Chim Acta 220:35
26. Kiyashkina ZS, Pomogailo AD, Kuzayev AI, Lagodzinskaya GV, Dyachkovskii FS (1980) Polymerization of acetylene monomers by molybdenum compounds fixed on the macromolecular supports. J Polym Sci Polym Symp 68:13
27. Jenkins DW, Hudson SM (2001) Review of vinyl graft copolymerization featuring recent advances toward controlled radical-based reactions and illustrated with chitin/chitosan trunk polymers. Chem Rev 101:3245–3274
28. Svec FJ (2010) Porous polymer monoliths: amazingly wide variety of techniques enabling their preparation. Chromatographia 1217: 902–924
29. Georgiev IG, MacGillivray LR (2007) Metal-mediated reactivity in the organic solid state: from self-assembled complexes to metal–organic frameworks. Chem Soc Rev 36:1239–1248
30. Batagin-Neto A, Bronze-Uhle ES, Fernandes DM, Fratoddi I, Venditti I, Decker F, Bodo E, Russo MV, Graeff CFO (2011) Optical behavior of conjugated Pt-containing polymetallaynes exposed to gamma-ray radiation doses. Phys Chem B 115:8047–8053
31. Gutzke ME, Yanco WH (1962) Radiation polymerization of acetylene derivatives; Monsanto Res. Corp.: United States Dept. Comm., Off. Techn. Serv., AD N. 297177
32. Tabata Y, Saito B, Shibano H, Sobue H, Oshima K (1964) Radiation-induced liquid- and solid-phase polymerization of acetylene. Macromol Chem Phys 76:89
33. Usanmaz A, Altürk E (2002) Radiation induced solid-state polymerization of acetylenedicaroxylic acid. J Macromol Sci Pure Appl Chem A39:379
34. Cataldo F, Strazzulla G, Iglesias-Groth S (2009) Synthesis of polyphenylacetylene by radiation-induced polymerization in deoxycholic acid clathrate. Radiat Phys Chem 78:244–250
35. Bassetti M, Fratoddi I, Lilla L, Pasquini C, Russo MV, Ursini O (2012) Synthesis of polyarylacetylenes by γ-ray-induced polymerization of terminal alkynes. Nanostructures of ortho-substituted derivatives. J Polym Sci A Polym Chem 50:5097–5106
36. Scherf U, Gutacker A, Koenen N (2008) All-conjugated block copolymers. Acc Chem Res 41(9):1086
37. Scherf U, Adamczyk S, Gutacker A, Koenen N (2009) All-conjugated, rod-rod block copolymers-generation and self-assembly properties. Macromol Rapid Comm 30:1059–1065
38. Fielding LA, Derry MJ, Ladmiral V, Rosselgong J, Rodrigues AM, Ratcliffe LPD, Sugihara S, Armes SP (2013) RAFT dispersion polymerization in non-polar solvents: facile production of block copolymer spheres, worms and vesicles in n-alkanes. Chem Sci 4: 2081
39. Charleux B, Delaittre G, Rieger J, D'Agosto F (2012) Polymerization-induced self-assembly: from soluble macromolecules to block copolymer nano-objects in one step. Macromolecules 45:6753–6765
40. Nyquist RA (1971) Vibrational assignments of H-C≡C-CH2OH and its deuterium analogs. Spectrochim Acta 27A:2513
41. Dong J, Ozaki Y, Nakashima K (1997) FTIR studies of conformational energies of poly (acrylic acid) in cast films. J Polym Sci B Polym Phys 35.3:507–515
42. Moharram MA, Khafagi MG (2007) Application of FTIR spectroscopy for structural characterization of ternary poly (acrylic acid)–metal–poly (vinyl pyrrolidone) complexes. J Appl Polym Sci 105(4):1888–1893
43. Yang M, Sun H, Chen W (1995) Simultaneous polymerization and formation of poly(propargyl alcohol) films by a novel palladium catalyst. Polym J 27:928–933
44. Zielhuis SW, Nijsen JFW, Dorland L, Krijger GC, van het Schip AD, Hennink WE (2016) Removal of chloroform from biodegradable therapeutic microspheres by radiolysis. Int J Pharm 315:67
45. Wolfe DH (1960) Method of making propargyl chloride, U.S. Patent 2,926,204
46. Williams TF (1971) Radiation-induced ionic polymerization controlled by the presence of Lewis acids or Lewis bases, U.S. Patent 3616369
47. Hayon E, Hayashi N, Ibata T, Lichtin NN, Matsumoto A (1971) Pulse radiolysis of liquid amides. J Phys Chem 75:2267–2272
48. Pukhalskaya GV, Kotov AG, Ya Pshezhetskii S (1969) The photochemistry of free radicals. The action of light on radicals in *gamma* irradiated formamide and imethylformamide. Khim Vysok Energii 3:340
49. Tran-Thi TH, Koulkes-Pujo AM (1983) Electron and organic radical anion solvation. Pulse radiolysis of tetrahydrofuran and its solutions of N-methylacetamide or pyrrolidone. J Phys Chem 87: 1166–1169
50. Colebourne N, Collinson E, Dainton FS (1963) 60 CO γ-radiolysis of N, N-dimethylformamide. Trans Faraday Soc 59:886
51. Tsuda Y (1962) Copolymerization studies of radiation-induced polymerization at low temperature. J Polym Sci 58:289–297
52. Ault BS, Andrews L (1975) Proton radiolysis of CHCl3and CHBr3at high dilution in argon during condensation at 15 °K. Infrared spectra of the CHX+2, CHX−2, and CHX−3molecular ions. J Chem Phys 63:1411–1418
53. Abadie MJM (1982) Radiolysis of liquid chloroform in an oxygen free atmosphere. Radiat Phys Chem 19:63
54. Kawahara S, Tsuzuki S, Uchimaru T (2005) Lewis acidity/basicity of π-electron systems: theoretical study of a molecular interaction between a π system and a Lewis acid/base. Chem Eur J 11:4458–4464
55. Fujita M, Ishida A, Majima T, Takamuku S (1996) Lifetimes of radical anions of dicyanoanthracene, phenazine, and anthraquinone in the excited state from the selective electron-transfer quenching. J Phys Chem 100:5382–5387
56. Hayashi N, Hayon E, Ibata T, Lichtin NN, Matsumoto A (1971) Pulse radiolysis of liquid amides. J Phys Chem 76:2267
57. Jasien PG, Weber LL (2001) A CIS study of solvent effects on the electronic absorption spectrum of Reichardt's dye. J Mol Struct THEOCHEM 572:203–212
58. Yang L, Jamal R, Liu F, Wang Y, Abdiryim T (2017) Structure and photocatalytic activity of a low band gap donor–acceptor–donor (D–A–D) type conjugated polymer: poly(EDOT–pyridazine–EDOT). RSC Adv 7:1877–1886
59. Guo X, Baumgarten M, Müllen K (2013) Designing π-conjugated polymers for organic electronics. Prog Polym Sci 38:1832–1908

60. Jang SH, Son TK (2014) Synthesis and characterization of a polyacetylene derivative with hydroxy functional groups. Mol Cryst Liq Cryst 597:153–158
61. Gal YS, Jin SH, Park YI, Park JW, Lyoo W, Lim KT, Kim SY (2011) Electro-optical and electrochemical properties of poly(1-hexyne). Fibers Polym 12:291–295
62. Zhang W, Tabei J, Shiotsuki M, Masuda T (2006) Synthesis of poly(propargyl esters) with rhodium catalysts and their characterization. Polym Bull 57:463–472
63. Tauc J, Menth A, Wood D (1970) Optical and magnetic investigations of the localized states in semiconducting glasses. Phys Rev Lett 25:749–752
64. Dai L, Li J, Yamada E (2002) Effect of glycerin on structure transition of PVA/SF blends. J Appl Polym Sci 86:2342–2347
65. Akram M, Taha I, Ghobashy MM (2016) Low temperature pyrolysis of carboxymethylcellulose. Cellulose 23:1713–1724
66. Geiss RH, Street GB, Volksen W, Economy J (1983) Polymer structure determination using electron diffraction techniques. IBM J Res Dev 27:321–329
67. Masuda T, Higashimura T (1987) Polyacetylenes with substituents: their synthesis and properties. Adv Polym Sci 81:121
68. Gal YS, Lee WC, Kim SY, Park JW, Jin SH, Koh KN, Kim SH (2001) Synthesis and properties of poly-(2-ethynylpyridinium bromide) having propargyl side chains. J Polym Sci Part A Polym Chem 39:3151–3158
69. Gal YS, Jin SH, Gui TL, Lee HJ, Kim SY, Kim DW, Ko JM, Chun JH, Jang SH, Kim BS, Lee WC (2003) Polymerization of 4-Dimethylamino-N-propargylpyridinium bromide by transition metal catalysts. J Macromol Sci Pure Appl Chem A40:401
70. Stevens GC, Bloor D (1978) ESR studies of a diacetylene polymer I. Partially crystalline polymer extracts. Phys Status Solidi 45:483–491
71. Weinberger BR, Kaufer J, Pron A, Heeger AJ, MacDiarmid AG (1979) Magnetic susceptibility of doped polyacetylene. Phys Rev B 20:223
72. Weinberger BR, Ehrenfreund E, Pron A, Heeger AJ, MacDiarmid AG (1980) Electron spin resonance studies of magnetic soliton defects in polyacetylene. J Chem Phys 72:9
73. Akagi K (2007) Liquid crystalline conjugated polymers – synthesis and properties In: Ramamoorthy A (ed) Thermotropic liquid crystals. Springer, pp 249–275
74. Lee I-H, Amaladass P, Yoon K-Y, Shin S, Kim Y-J, Kim I, Lee E, Choi T-L (2013) Nanostar and nanonetwork crystals fabricated by in situ nanoparticlization of fully conjugated polythiophene diblock copolymers. J Am Chem Soc 135:17695–17698
75. Yoon K-Y, Lee I-H, Choi T-L (2014). RSC Adv 4:49180
76. Lee I-H, Choi T-L (2016) Importance of choosing the right polymerization method for in situ preparation of semiconducting nanoparticles from the P3HT block copolymer. Polym Chem 7:7135–7141
77. Lee I-H, Amaladass P, Choi TL (2014) One-pot synthesis of nanocaterpillar structures via in situ nanoparticlization of fully conjugated poly(p-phenylene)-block-polythiophene. Chem Commun 50:7945–7948
78. Shin S, Yoon K-Y, Choi T-L (2015) Simple preparation of various nanostructures viain situnanoparticlization of polyacetylene blocklike copolymers by one-shot polymerization. Macromolecules 48:1390–1397